Mon. Not. R. Astron. Soc. **000**, 1–?? (2012) Printed 12 September 2012 (MN LATEX style file v2.2)

Escape Fraction of Ionizing Radiation from Starburst Galaxies at High Redshifts

Andrea Ferrara[1] & Abraham Loeb[2]
[1] *Scuola Normale Superiore, Piazza dei Cavalieri 7, I-56126 Pisa, Italy*
[2] *Astronomy department, Harvard University, 60 Garden Street, Cambridge MA 02138, USA*

12 September 2012

ABSTRACT
Recent data indicates that the cosmic UV emissivity decreased with decreasing redshift z near the end of reionization. Lacking evidence for very massive early stars, this could signal a decline with time in the mass-averaged escape fraction of ionizing radiation from galaxies $\langle f_{esc}\rangle$ at $z \gtrsim 6$. We calculate the evolution of ionization fronts in dark matter halos which host gas in hydrostatic equilibrium at its cooling temperature floor ($T \approx 10^4$ K for atomic hydrogen). We find a high escape fraction only for the lowest mass halos (with $M < 10^{8.7}\,\mathrm{M}_\odot$ at $(1+z) = 10$) provided their star formation efficiency $f_\star \gtrsim 10^{-3}$. Since the low-mass galaxy population is depleted by radiative feedback, we find that indeed $\langle f_{esc}\rangle$ decreases with time during reionization.

Key words: Reionization, Galaxies, Star Formation

1 INTRODUCTION

The first generation of galaxies is expected to have reionized cosmic hydrogen by a redshift $z \approx 7$ (Loeb & Furlanetto 2013). One of the most important unknown parameters regulating the way in which reionization proceeds is the fraction of ionizing photons, f_{esc}, that escape outside the virial radius of the galaxies in which they were produced and into the surrounding intergalactic medium (IGM). The growth of ionized regions with cosmic time depends on the average value of this parameter over viewing angle per galaxy and over the galaxy population (Wyithe & Loeb 2003; Trac & Cen 2007; Bouwens et al. 2012; Finkelstein et al. 2012).

Observations of galaxies at $z = 1-3$ indicate a broad set of escape fraction values ranging from a few percent to tens of percent (Steidel et al. 2001; Fernández-Soto et al. 2003; Shapley et al. 2006; Inoue et al. 2006; Siana et al. 2007; Giallongo et al. 2008; Iwata et al. 2009; Boutsia et al. 2011; Grazian et al. 2011; Vanzella et al. 2012a,b). This potentially reflects strong variations of the escape fraction with viewing angle and evolutionary time.

A calculation of the escape fraction of ionizing radiation from first principles is difficult, as it depends on the spatial distribution of ionizing sources relative to the neutral hydrogen in galaxies and is therefore sensitive to the small scale clustering of young stars and the interstellar medium. Due to their higher density, high-redshift galactic disks are expected to have small escape fractions during reionization (Wood & Loeb 2000; Gnedin et al. 2008; Razoumov & Sommer-Larsen 2006; Wise & Cen 2009). Even for local disk galaxies, Dove et al. (2000) concluded that f_{esc} should not exceed a few percent in most cases, as a result of efficient radiation trapping by the shells of the expanding superbubbles around OB star associations.

Since the mean density of the Universe (and hence galaxies) scales as $(1+z)^3$, theoretical calculations tend to conclude that $f_{\rm esc}$ should decrease with increasing redshift. This expectation appears to be in conflict with recent reionization models and data (Bolton & Haehnelt 2007; Salvaterra et al. 2011; Mitra et al. 2012a,b; Kuhlen & Faucher-Giguère 2012; Finkelstein et al. 2012) that point towards the need for an increasing UV emissivity towards high redshifts. This can be achieved in two ways. The first is to postulate an increasingly top-heavy initial mass function (IMF) of stars that would increase the number of photons emitted per baryon incorporated in stars. Although possible, this explanation seems to be disfavored by the lack of observational evidence for an early population of substantially more massive stars (Cayrel et al. 2004; Caffau et al. 2011) and by recent numerical simulations (Greif et al. 2012). A more appealing solution is represented by a possible increase in the average escape fraction $\langle f_{\rm esc}\rangle$ during reionization, recently suggested by Mitra et al. (2012b). Here we explore a novel physical explanation for this unexpected trend.

We show that the lowest-mass galaxies near or below (so-called mini-halos) the hydrogen cooling threshold have high escape fractions but their contribution to the UV production rate decreases with cosmic time due to large-scale radiative feedback processes during reionization that either photo-heat or sterilize them by dissociating their H_2. How-

ever, internal feedback is of foremost importance as well: as these small systems achieved large f_{esc} by rapidly (within $\sim 10^4$ yr) ionizing their entire interstellar medium, this gas will become loosely bound to the host galaxy. Under these conditions it is difficult to sustain a continuous mode of star formation (SF), particularly because following the death of massive stars powerful supernova explosions will clear the gas out of the potential well before a stable disk structure is established. More massive galaxies will form a disk with the net result of trapping most of their ionizing photons.

If high-redshift dwarf galaxies form stars predominantly in episodic bursts, as suggested by the high incidence of galaxy mergers at increasing redshift (Muñoz & Loeb 2011), the conventional argument that their star formation efficiency is suppressed by supernova (SN) feedback may not be valid. In particular, SN feedback is inhibited if the duration of the starburst is shorter than ~ 10 Myr, the lifetime of SN progenitors. In this regime, the global radiative feedback sets the amount of gas initially available for making stars and hence the overall efficiency of star formation, $f_\star$. In our calculations, we will calibrate the value of $f_\star$ based on recent measurements of the cosmic stellar mass density at high redshifts (González et al. 2011).

For an instanteneous starburst, $f_{\rm esc}$ can be large only if an escape route for ionizing photons is opened within a few Myr, prior to the death of the massive stars that produce these photons. This process cannot be mediated by supernova explosions, which occur after the emission of ionizing photons has already started to decline. The key question is therefore whether the surrounding blanket of absorbing hydrogen atoms can be ionized before the massive stars in the starburst end their life. We address this question within the context of a simple model in which we populate dark matter halos with primordial gas that cooled to the temperature floor of atomic hydrogen, $\sim 10^4$K.

Our basic point is simple: massive galaxies exist at all redshifts and the escape fraction of ionizing radiation from them is calculated and observed to be small; however, the lowest-mass galaxies ($T_{vir} \lesssim 10^4$ K) exist only before and during reionization and have a high f_{esc}. Our assumption of a short-lived star formation phase without SN feedback is self-consistent, as we will show that photoionization heating of the gas suppresses star formation in dwarf galaxies after a period of time much shorter than the lifetime of massive stars.

In §2 we describe the details of our calculation and in §3 we present our numerical results. Finally, we discuss our main conclusions in §4. Throughout the paper, we adopt the WMAP7 set of cosmological parameters with $\Omega_m = 0.27$, $\Omega_\Lambda = 1-\Omega_m$, $\Omega_b h^2 = 0.023$, $h = 0.71$, $\sigma_8 = 0.81$, $n_s = 0.97$, and ${\rm d}n_s/{\rm d}\ln k = 0$ (Larson et al. 2011).

2 METHOD OF CALCULATION

We derive the escape faction of the ionizing photons, f_{esc}, based on a set of simplifying assumptions. We consider a spherical dark matter halo of mass, M, virializing at redshift z and characterized by an internal density (spherically averaged) profile following the Navarro-Frenk-White (Navarro et al. (1997), NFW) form,

$$\rho(r) = \frac{\rho_c \delta_c}{cx(1+cx)^2}, \quad (1)$$

where $x \equiv r/r_{vir}$, r_{vir} is the virial radius of the system, c is the halo concentration parameter, $\delta_c = (18\pi^2/3)c^3/F(c)$ is a characteristic overdensity, and

$$F(t) = \ln(1+t) - \frac{t}{1+t}. \quad (2)$$

For the concentration parameter we use the results of Prada et al. (2012), extrapolating them towards lower masses and higher redshift when necessary. The circular velocity, $v_c^2(r) = GM(r)/r$, can be expressed as

$$v_c^2 = V_c^2 \frac{F(cx)}{xF(c)}, \quad (3)$$

with $V_c^2 \equiv GM/r_{vir}$. Baryons fall into the dark matter halo potential well are shock-heated to the virial temperature $T_{vir} = (\mu m_p/2k)V_c^2$, and then relax to a hydrostatic configuration (Makino et al. 1998),

$$\ln \rho(r) = \ln \rho_0 - \frac{V^2}{V_c^2}[v_e^2(r=0) - v_e^2(r)]. \quad (4)$$

Here, v_e is the halo escape velocity from the halo,

$$v_e^2(r) = 2V_c^2 \frac{F(cx) + cx/(1+cx)}{xF(c)}; \quad (5)$$

$\mu = 1.22$ is the mean molecular weight of a neutral primordial H-He gas; k_B is the Boltzmann constant and m_p the proton mass. We have also inserted in equation (4) the extra factor $V^2 = V_c^2/c_s^2 = T_{vir}/T > 1$, where $c_s^2 = 2k_B T/\mu m_p$ is the effective sound speed at a generic temperature $T \neq T_{vir}$. The standard case in which $T = T_{vir}$ is obtained by setting $V = 1$. By manipulating equation (4) we then get the final expression for the gas density profile as a function of radius,

$$\rho(x) = \rho_0 e^{-\gamma^2 V^2}(1+cx)^{\gamma^2 V^2/cx} \equiv \mu m_p n_0 \eta(x); \quad (6)$$

where we have defined $\gamma^2 = 2c/F(c)$, and the ancillary function $\eta(x) = e^{-\gamma^2 V^2}(1+cx)^{\gamma^2 V^2/cx}$. The central density, ρ_0, is obtained by requiring that the total gas mass in the halo is equal to the cosmological value, i.e. $M_b = (\Omega_b/\Omega_m)M = f_b M$. This procedure yields

$$\rho_0 = (18\pi^2/3) f_b c^3 e^{\gamma^2 V^2} \left[\int_0^c dt (1+t)^{\gamma^2 V^2/t} t^2\right]^{-1}, \quad (7)$$

Table 1 provides the values of the central number density, n_0, for different halo masses and V values at a fixed redshift, $z = 9$. As expected, n_0 increases in larger masses even

Table 1. Values of central number density, n_0 (in units of cm^{-3}) for dark matter halos of different total mass, M, at $z = 9$ and for different values of the gas temperature, T, expressed in terms of the virial temperature T_{vir} through the parameter $V^2 = T_{vir}/T$.

$\log_{10} T_{vir}$ [K]	4.31	4.98	5.65	6.32
M [M$_\odot$]	10^8	10^9	10^{10}	10^{11}
$V^2 = 1.0$	20.6	23.9	36.0	167.8
$V^2 = 1.2$	46.2	54.5	87.3	282.9
$T = 2 \times 10^4$ K	24.3	1.9×10^4	4.3×10^6	—

in the case $V = 1$ in which the gas is at the virial temperature of the halo. This reflects the strong dependence of n_0 on the concentration parameter, which increases from $c \approx 4$ for $M = 10^8\,\mathrm{M}_\odot$ to $c \approx 6.5$ for $M = 10^{11}\,\mathrm{M}_\odot$. This increasing trend is amplified if the gas is cooler than the virial temperature ($V > 1$) or if it is thermostated at a fixed temperature (such as $T = 2 \times 10^4$ K in Table 1), leading to unrealistic densities for the most massive halos with $M = 10^{11}\,\mathrm{M}_\odot$ (which represent rare 3σ fluctuations of the density field at $z = 9$). For massive halos we obtain artificially high densities because we ignore angular momentum. Once the gas condenses to a sufficiently small scale, its rotation will halt contraction and it will settle to a disk. Disks were considered by Wood & Loeb (2000) and Dove et al. (2000) who independently concluded that the escape fraction was negligible for a smooth gas distribution in high-redshift disks and also local spirals. We therefore argue that once the gas contracts enough to make a disk, its density will not increase by as much as our spherical model predicts but UV photons will not be able to escape from it anyway, based on earlier studies.

2.1 Ionization front evolution

Having specified the gas density distribution inside halos, we may now derive the evolution of an ionization front (IF) driven by the emission of photons with energy > 13.6eV from a burst of star formation at the halo center. We assume that a fraction $f_\star$ of the available gas, $f_b M$, of a given halo is instantaneously converted into stars distributed in mass according to a Salpeter IMF in the range $(m_{low}, m_{up}) = (1\,\mathrm{M}_\odot, 100\,\mathrm{M}_\odot)$ and with absolute metallicity $Z = 10^{-3}$. The ionizing photon production rate, $Q(t)$, by the stellar cluster can be computed exactly from population synthesis models: we use here `Starburst99`[1] Leitherer et al. (1999). The time dependence of the production rate of ionizing photons rate under these conditions is,

$$Q(t) = \frac{Q_0}{1 + (t/t_0)^4}, \tag{8}$$

with $(Q_0, t_0) = (10^{47}\mathrm{s}^{-1}\,{\mathrm{M}_\odot}^{-1}, 10^{6.6}\ \mathrm{yr})$. Equation (8) illustrates the important point that after ~ 40 Myr, the production rate of ionizing photons rapidly drops as a result of the death of short-lived massive stars. This has important implications for f_{esc} as discussed hereafter. Note that equation (8) implies that the number of ionizing photons emitted per baryon incorporated into stars is $N_\gamma \approx 0.5 Q t_0 m_p/\,\mathrm{M}_\odot = 5 \times 10^3$.

The time evolution of the IF radius, r_I, is described by an ordinary differential equation that expresses a detailed balance between the ionization and recombination rates within the volume enclosed by the IF,

$$\frac{dr_I}{dt} = \frac{1}{4\pi n_H r_I^2}\left[Q(t) - \frac{4\pi}{3} r_I^3 n_H^2 \alpha^{(2)}\right], \tag{9}$$

where $n_H = 0.92n$ is the hydrogen density for a primordial gas and $\alpha^{(2)} = 2.6 \times 10^{-13}(T/10^4\mathrm{K})^{-1/2}$ is the Case B recombination rate of hydrogen (Maselli et al. 2003). Normalizing by an effective recombination rate in the halo, $\dot{\mathcal{N}}_{rec} = (4\pi/3)\alpha^{(2)} n_{H0}^2 r_{vir}^3$, and adopting a dimensionless time variable $\tau = t/t_{rec} = \alpha^{(2)} n_{H0} t$, equation (9) can be written in a dimensionless form,

$$\frac{dx}{d\tau} = \frac{Q(t)}{3\dot{\mathcal{N}}_{rec}\eta(x)x^2} - \frac{1}{3}x\eta(x). \tag{10}$$

Equation (10) describes the expansion of the H II region into the stratified gas distribution within the halo. As the density decreases outwards, the IF accelerates and eventually exits the virial radius at a time $t_{out} \equiv t(x = 1)$. Until t_{out} all the ionizing photons are absorbed inside the halo[2]; hence, $f_{esc} \approx 0$. However, for $t > t_{out}$, ionizing photons will be only used *to keep* the halo ionized by balancing recombinations within it, but a large fraction of them will be able to escape into the IGM, thus making $f_{esc} > 0$. We then express the net escape fraction as follows:

$$f_{esc} = \frac{\int_{\tau(x=1)}^{\infty} d\tau Q(t)}{\int_0^\infty d\tau Q(t)}. \tag{11}$$

As we will see shortly, though, either the IF is efficiently confined by the density, $dx/d\tau \to 0$, or the blow out will occur on a very short time scale thus making $f_{esc} \approx 1$. We will refer to these two different situations as a "confined" or "unconfined" IF in the rest of the paper.

3 RESULTS

We solved numerically equation (10) for a number of halo masses with $V = 1$ in the range $M = 10^8$–$10^{11}\,\mathrm{M}_\odot$ at two selected redshifts, $z = 9$ and $z = 14$. Figures 1 and 2 show the results for $f_\star = 0.2\%$, a natural value for for nearly primordial star-forming halos (Barkana & Loeb 2001; Ciardi & Ferrara 2005).

IFs in these early halos evolve rapidly to the strong radiative input by the stars and reach a radius $r_I = r_{vir}$ within ~ 1 Myr, yielding $f_{esc} = 0.98 - 0.90$ for halo masses up to $M \approx 2 \times 10^{10}\,\mathrm{M}_\odot$, beyond which the IF is confined within the halo, and hence $f_{esc} = 0$. It requires fine tuning for a single object to achieve intermediate f_{esc} values; rather, the process favors on-off states implying that the escape fraction of photons from galaxies can be intermittent: depending on variations of $f_\star$ in different bursts (say, due to the increasing gas metallicity or decreasing gas fraction due to mass loss from supernova-driven winds) the same halo might switch from being dark to bright above the Lyman limit. Note also that for the largest IF-confined halos, the H II region starts to shrink at $t \gtrsim 3$ Myr as a result of recombinations and the decline in the supply rate of ionizing photons.

The situation is dramatically different at $z = 14$ (for the same $f_\star$): at that epoch all halos confine their IF and have $f_{esc} = 0$. This is due to the increase in the gas density and the larger concentration factor at a fixed mass. A more global view of the dependence of f_{esc} on halo mass and star formation efficiency at $z = 9$ is given by Fig. 3. The abrupt transition from $f_{esc} \approx 1$ to zero is very weakly dependent on halo mass, except for the narrow range of $-2.8 < \log f_\star < -2.2$ in which larger halos tend to be more

[1] http://www.stsci.edu/science/starburst99/

[2] Here we ignore the possibility of a highly inhomogeneous medium in which low density channels for escape exist.

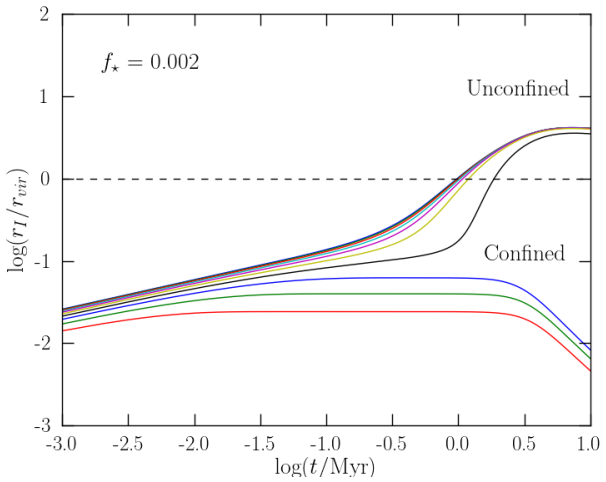

Figure 1. Time evolution of the ionization front radius, r_I, at $z = 9$ within halos of different total mass $M = 10^{8.+j/3}\,\mathrm{M}_\odot$, with $j = 0, .., 9$ from the top curve ($M = 10^8\,\mathrm{M}_\odot$) to the bottom one ($M = 10^{11}\,\mathrm{M}_\odot$). The assumed star formation efficiency is $f_\star = 0.002$ and the gas temperature factor $V = (T_{vir}/T)^{1/2} = 1$.

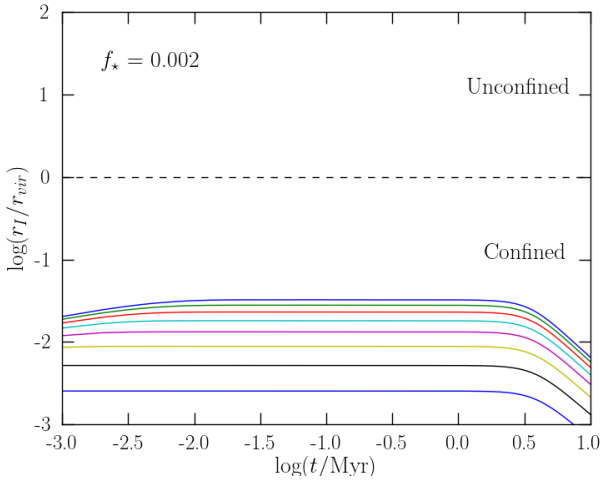

Figure 2. Same as Fig. 1, but for $z = 14$.

opaque to ionizing photons. Above this range, $f_{esc} = 1$ independently of halo mass and star formation efficiency, and below this range, $f_{esc} = 0$.

Figure 4 shows the examples with $V > 1$ introduced in Table 1, for which $T = 2 \times 10^4$ K, corresponding to $V^2 = (1.04, 4.82, 22.39, 103.96)$ for halos of mass $M/\,\mathrm{M}_\odot = (10^8, 10^9, 10^{10}, 10^{11})$ and hence resulting in considerably denser and more compact gas configurations. The IF front is now largely confined within all halos with $M > 10^8\,\mathrm{M}_\odot$ even if the star formation efficiency has been increased by a factor of 50 with respect to the case with $V = 1$ shown in Fig. 1. In addition, the IF escapes the virial radius in a very short time[3], $t_{out} \sim 10^4$ yr.

The different behavior relative to the case of $V = 1$ is

[3] We have checked that the IF speed is subluminal, $dr_I/dt < c$

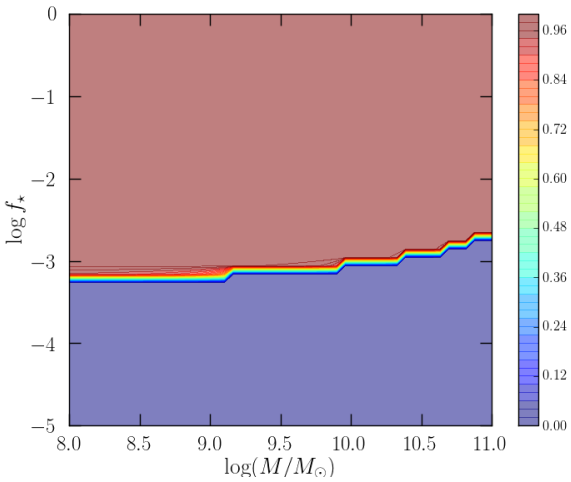

Figure 3. Map of f_{esc} values as a function of halo mass and star formation efficiency at $z = 9$ assuming $V = (T_{vir}/T)^{1/2} = 1$. The color scheme defined by the vertical bar on the right hand side.

caused by the associated high gas density (see Table 1). The small scale height of the gas distribution, correspondingly reduced by a analogous factor $\propto V^2$, forces the steep acceleration seen just prior to blow out. In analogy with the $V = 1$ case, we show the dependence of f_{esc} on halo mass and star formation efficiency at $z = 9$ (Fig. 5). In this case the $f_{esc} = 1$ area is much narrower and limited to small halos with $M < 10^{8.7}\,\mathrm{M}_\odot$ and $f_\star \gtrsim 10^{-3}$. Thus, according to our model, it is only the smallest halos that are truly able to inject ionizing photons in the IGM and therefore substantially contribute to reionization. Larger halos are instead able to confine their H II regions very effectively. At $z = 14$ the $f_{esc} = 1$ region is qualitatively the same, but its area shrinks because of the larger background density and the increased concentration parameter at a fixed halo mass.

The existence of a minimum value of $f_\star \approx 10^{-3}$ to allow the escape of photons can be understood based on a simple argument. This minimum number of ionizing photons provided to each hydrogen atom in the halo must balance the number of recombinations it undergoes during the lifetime of the starburst, approximately equal to $t_0 = 10^{6.6}$ yr (see equation 8). This can be expressed by the following inequality:

$$f_\star \geqslant \frac{C}{\mathcal{N}_\gamma}\frac{\alpha^{(2)}t_0}{\mu m_p}(18\pi^2)\Omega_b\rho_c(z) \quad (12)$$

$$= 0.7\times10^{-3}\left(\frac{C}{3}\right)\left(\frac{5\times10^3}{\mathcal{N}_\gamma}\right)\left(\frac{1+z}{10}\right)^3, \quad (13)$$

where $C = \langle n_H^2\rangle/\langle n_H\rangle^2 \approx 3$ is the clumping factor accounting for the gas density structure inside a NFW halo.

The results for halos with $M \lesssim 10^8\,\mathrm{M}_\odot$ in which $T_{vir} \lesssim 2 \times 10^4$ K at $z = 9$ need some extra attention. In fact, by fixing the gas temperature to 2×10^4K, the gas might have never been accreted in the first place; this is the case if for example the halo is located within an already ionized region. To correct this problem, we have set $V = 1$ in these mini-halos; of course, this requires that some cooling agent, such as H_2 , HD or LiH, would cool the gas in these systems to make stars.

Table 2. Values of various quantities related to the global evolution of the mass-averaged escape fraction. See text for more details.

	Mass-averaged f_{esc} – Constant $f_\star$						
	M_{sf} [$M_\odot$]	M_{f1} [$M_\odot$]	M_{f0} [$M_\odot$]	$f_{coll}(>M_{sf})$	$f_{coll}(>M_{f0})$	$\langle f_{esc}\rangle$	$f_\star$
$z=6$	2.977e+08	2.977e+08	4.852e+08	1.379e-01	1.262e-01	8.478e-02	3.000e-02
$z=9$	1.169e+07	1.169e+07	2.190e+08	1.130e-01	5.936e-02	4.747e-01	3.000e-02
$z=9$	1.169e+07	1.169e+07	5.818e+08	1.130e-01	4.374e-02	6.130e-01	1.000e+00
$z=9$	1.169e+07	1.169e+07	1.169e+07	1.130e-01	1.130e-01	0.000e+00	1.000e-04
$z=14$	1.634e+06	1.634e+06	8.131e+07	5.373e-02	1.471e-02	7.263e-01	3.000e-02
	Mass-averaged f_{esc} – Variable $f_\star(z)$						
	M_{sf} [$M_\odot$]	M_{f1} [$M_\odot$]	M_{f0} [$M_\odot$]	$f_{coll}(>M_{sf})$	$f_{coll}(>M_{f0})$	$\langle f_{esc}\rangle$	$f_\star$
$z=8$	5.361e+07	5.361e+07	1.527e+08	1.098e-01	8.866e-02	1.924e-01	2.192e-03
$z=10$	3.664e+06	3.186e+07	7.361e+07	7.232e-02	5.866e-02	1.889e-01	1.296e-03
$z=12$	2.030e+06	2.030e+06	2.030e+06	8.003e-02	8.003e-02	0.000e+00	1.156e-03

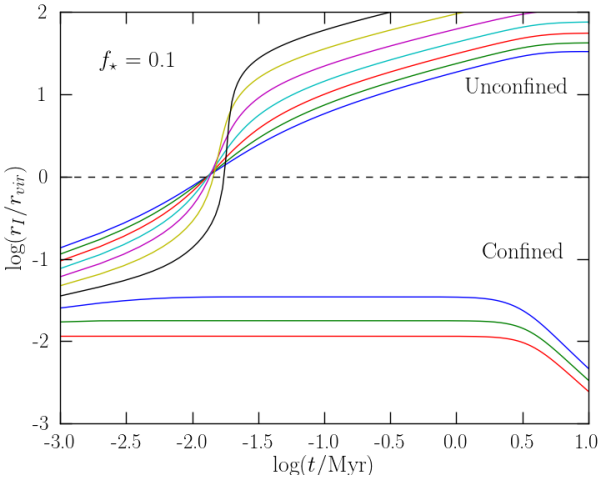

Figure 4. Same as Fig. 1, but for halos with mass in the range $M = 10^{8.+2j/30}\,M_\odot$, with $j = 0,..,9$ from the top curve ($M = 10^8\,M_\odot$) to the bottom one ($M = 3\times10^8\,M_\odot$). The star formation efficiency is $f_\star = 0.1$ and the gas temperature has been fixed to $T = 2\times10^4$ K, giving a variable V temperature factor (see text for details).

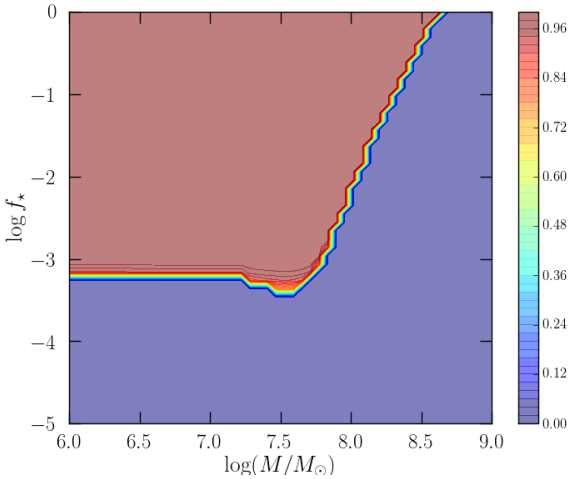

Figure 5. Same as Fig. 3 but for a fixed gas temperature $T = 2\times10^4$ K.

3.1 Global redshift evolution

Next we would like to constrain the redshift evolution of $f_{esc}(z)$ when averaged over the entire galaxy population.

The dark matter halo mass function, $n(M,z)$, is well described by the Sheth & Tormen (2002) form:

$$n(M,z)dM = A\left(1+\frac{1}{\nu'^{2q}}\right)\sqrt{\frac{2}{\pi}}\frac{\bar{\rho}}{M}\frac{d\nu'}{dM}\exp\left(-\frac{\nu'^2}{2}\right)dM, \quad (14)$$

with $A = 0.322$, $q = 0.3$, $\nu' = \sqrt{a}\nu$, $a = 0.707$, $\nu = \delta_c/D(z)\sigma(M)$, with $\delta_c = 1.686$, $D(z)$ being the linear growth factor and $\sigma(M)$ being the r.m.s. amplitude of density fluctuations on a mass scale M.

We define the mass-averaged escape fraction, $\langle f_{esc}\rangle$ at a given $f_\star$ and redshift z as follows:

$$\langle f_{esc}\rangle(z,f_\star) = 1 - \frac{F\,[>M_{f0}(z,f_\star)]}{F\,[>M_{sf}(z)]}, \quad (15)$$

where $F(>M,z) = \int_M^\infty nMdM/\int_0^\infty nMdM$ is the collapse fraction of all matter in haloes with mass exceeding M at redshift z.

Equation (15) contains two important characteristic masses. The first, $M_{f0}(z,f_\star)$, is defined as the halo mass above which, for a given redshift z and star formation efficiency $f_\star$, no ionizing photons can escape, i.e. $f_{esc} = 0$. The results presented above allow us to precisely determine $M_{f0}(z,f_\star)$.

The second mass scale, $M_{sf}(z)$, denotes the redshift-dependent minimum mass of star-forming haloes which is set by radiative feedback. The evolution of M_{sf} is determined by two distinct radiative feedback processes. The first one is related to the increase of the cosmological Jeans mass in progressively ionized cosmic regions; as a result, the infall of gas in haloes below a given virial temperature is quenched. The evolution of $M_{sf}(z)$ depends on the details of the reion-

ization history (Gnedin 2000; Okamoto et al. 2008; Schneider et al. 2008). Guided by these findings, we adopt the the value $M_{sf} = M(T_{vir} = T_2)$ with $T_2 = 3 \times 10^4$ K after the end of reionization, here assumed to occur at $z_{rei} = 6$.

Before reionization (at least in the mostly neutral regions) a second type of feedback, involving the photodissociation of H_2 molecules by the Lyman-Werner (LW) background photons, becomes important. As H_2 is the primary coolant for minihalos ($T_{vir} < 10^4$ K), fragmentation of the gas to stars could be suppressed in these objects through H_2 dissociation by the UV background (Haiman et al. 1996; Ciardi et al. 2000; Kitayama et al. 2000; Machacek et al. 2001). According to Dijkstra et al. (2004), $z \sim 10$ minihalos with $T_{vir} = T_1 \approx 2 \times 10^3$ K can self-shield H_2 and cool, hence we use this value as the lower threshold for star formation. During reionization the interplay between the photoionization heating and LW-feedback is complicated (see the discussion in Mesinger & Dijkstra (2008) and Fig. 25 of Ciardi & Ferrara (2005)) and and the evolution of M_{sf} during this epochs is uncertain. To circumvent this uncertainty, we follow the phenomenological approach of Salvadori & Ferrara (2009) and Salvadori & Ferrara (2012) who suggested that the metallicity distribution and iron-luminosity relation of the Ultra Faint dSphs in the Milky Way halo can be explained if these objects are relic mini-halos that formed their stars prior to reionization. With this perspective, one can reconstruct $M_{sf}(z)$ by fitting local data. This approach yields the functional form,

$$M_{sf}(z) = M[T_{vir} = (T_2 - T_1)e^{(z-z_{rei})^2/\Delta z} + T_1], \quad (16)$$

with $\Delta z = 4$, which we adopt here.

In general $M_{f0}(z, f_\star) > M_{sf}(z)$. However, for sufficiently low values of $f_\star$, $M_{f0}(z, f_\star) = M_{sf}(z)$ and $\langle f_{esc} \rangle = 0$. To illustrate this point (see Table 2), we examine the results at $z = 9$ in Figure 5. For $f_\star = 0.03$, stars are formed only in halos more massive than $M_{sf} = 1.17 \times 10^7\,M_\odot$. Ionizing photons can only escape from halos less massive than $M_{f0} = 2.19 \times 10^8\,M_\odot$. As a result, there is a narrow range of objects that contribute to the ionizing photons budget in the IGM. Below that range stars cannot form and above it the gas is sufficiently dense to confine the H II region. When weighted with the halo mass function, though, the collapsed mass fraction above (M_{sf}, M_{f0}) is $(0.113, 0.059)$, yielding the large value $\langle f_{esc} \rangle (z = 9, f_\star = 0.01) = 0.847$. Since H II regions in abundant low mass halos are unbound, the average escape fraction is high. The width of the range progressively shrinks as star formation becomes less efficient. This is evident from Table 2, where for $z = 9$ and $f_\star = 10^{-4}$, $M_{f0}(z, f_\star) = M_{sf}(z)$ and the escape fraction drops to zero. These results underline the importance of the possible evolution in the star formation efficiency, which we address below.

The redshift evolution of the results can be understood in terms of a balance between two opposite trends. On the one hand, the halo central densities tend to become larger with increasing redshift, providing a more efficient confinement of the IF and acting to decrease $\langle f_{esc} \rangle$. On the other hand, more dwarf galaxies and mini-halos are able to produce ionizing photons as the critical mass M_{sf} decreases with increasing z. The overall evolution for the two specific values $f_\star = (0.03, 0.003)$ can be seen in Figure 6 (solid curves). For the high $f_\star$ case, the escape fraction continues

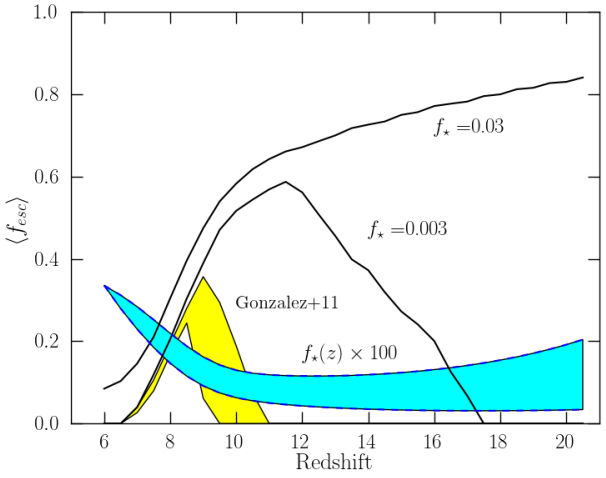

Figure 6. Redshift evolution of the mass-averaged escape fraction for different assumptions concerning the star formation efficiency. Solid lines refer to the redshift-independent values $f_\star = 0.03, 0.003$ as indicated by labels; the shaded area refers to $f_\star(z)$ (shown by the shaded cyan area and multiplied by a factor 100) derived from the stellar mass density evolution by González et al. (2011) based on equation (17).

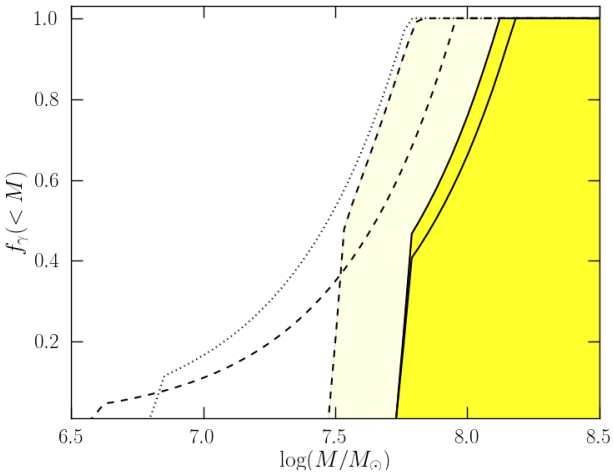

Figure 7. Cumulative fraction of ionizing photons produced by halos below a given halo mass M. Lines refer to a constant star formation efficiency $f_\star = 0.003$; shaded regions refer to the upper limit of the redshift-dependent $f_\star$ (equation 17) based on González et al. (2011) SMDs. For both sets of curves, solid (dashed) lines refer to $z = 8$ ($z = 10$); for $f_\star = 0.003$ the case for $z = 12$ (dotted) is also shown.

to increase with redshift, reaching $\langle f_{esc} \rangle = 0.83$ at $z = 20$. If instead $f_\star = 0.003$, the escape fraction reaches a peak value of 0.59 at $z = 11.5$ where it starts to decrease until it reaches zero at $z = 17.5$ when the density effect dominates over the enhanced photon production rate. Interestingly, a nearly redshift-independent $f_\star$ above a threshold of $\approx 0.1\%$ (see Fig. 5) always leads to $d\langle f_{esc} \rangle / dz > 0$ during the final phase of reionization. Although a rather weak mass dependence of $f_\star$ for galaxies of stellar mass $M_\star > 3 \times 10^7\,M_\odot$ is

inferred from local SDSS data (Dekel & Woo 2003), there are indications of a decreasing star formation efficiency for high-z galaxies. Recently, different groups (Stark et al. 2009; Labbé et al. 2010; González et al. 2011) have obtained stellar masses of galaxies in the redshift range $4 < z < 7$ from spectral energy distribution fitting to rest-frame optical and UV fluxes from Hubble-WFC3/IR camera observations of the Early Release Science field combined with the deep GOODS-S Spitzer/IRAC data. From this data it has been possible to reconstruct (see Fig. 4 of González et al. (2011)) the evolution of the comoving Stellar Mass Density (SMD), which we define here as $\rho_\star(z)$. The main result is that $\rho_\star(z=6) = 10^7\,\mathrm{M}_\odot\ \mathrm{Mpc}^{-3}$; in addition, the SMD grows with decreasing redshift as $\propto (1+z)^{-3.4\pm0.8}$. We can exploit this observational result to obtain a robust estimate for $f_\star(z)$ based on the relation,

$$f_\star(z) = \frac{\rho_\star(z)}{f_b F\left[>M_{sf}(z)\right]\rho_c}. \quad (17)$$

In other words, we tune the star formation efficiency so that baryons in collapsed halos account for the abundance of stars observed at $z < 7$. Note that the González et al. (2011) SMD has also been corrected for incompleteness at low masses. The range of allowed values of $f_\star$ implied by the data and obtained through equation (17) are plotted as a shaded area in Fig. 6. The data suggest $f_\star = 0.003$ at $z = 6$ (for display reasons we have multiplied the values by a factor 100 in the Figure) decreasing thereafter by a factor of about three above $z = 10$.

The main consequence of a suppressed star formation efficiency in low mass objects is to introduce a new intermediate mass scale $M_{sf} < M_{f1} < M_{f0}$ such that $f_{esc} > 0$ only in the interval $[M_{f1}, M_{f0}]$. Stated differently, this is an evidence of the fact that even objects that are above M_{sf} and can form stars, are now more efficient at confining their IFs; therefore their escape fraction becomes zero. Table 2 shows how M_{f1} gradually approaches M_{f0} towards high redshifts, closing the non-vanishing escape fraction window.

Another interesting question is how the global production of ionizing photons is distributed among halos of different masses. We quantify this through the cumulative fraction of ionizing photons produced by halos below a given mass,

$$f_\gamma(<M,z) \propto \int_{M_{sf}}^{M} f_{esc}(M',z,f_\star) f_\star(M_{sf},z) M' dM', \quad (18)$$

as shown in Figure 7. Due to their large escape fraction, halos with masses $M \lesssim 10^8\,\mathrm{M}_\odot$ are the dominant contributors to the cosmic ionizing photon budget. This holds for the more realistic redshift-dependent $f_\star$, but also for the constant $f_\star$ case. Thus, the low-mass galaxies and mini-halos might have dominated reionization. In particular, at $z = 10$ the mass corresponding to $T = 10^4$ K limiting the mini-halo mass range from above, is $\sim 3\times10^7\,\mathrm{M}_\odot$. Figure 7 shows that independently of the star formation efficiency prescription, we predict that mini-halos contribute $\sim 40\%$ of the total emissivity.

Reionization models suggest an increasing emissivity towards high redshifts (Bolton & Haehnelt 2007; Mitra et al. 2012a,b; Kuhlen & Faucher-Giguère 2012), whose most natural explanation is in terms of a f_{esc} increasing with redshift as we find here. For example, Mitra et al. (2012b) find that: *(i)* the escape fraction increases from $\langle f_{esc}\rangle = 0.068^{+0.054}_{-0.047}$ at z=6 to $0.179^{+0.331}_{-0.132}$ at $z = 8$; and *(ii)* at $z = 10$ $\langle f_{esc}\rangle > 0.146$.

4 DISCUSSION

We have calculated the escape fraction of ionizing photons from starburst galaxies during reionization, assuming that galactic gas cools down to a temperature floor ($\sim 10^4$K for atomic hydrogen and $\sim 2\times10^3$K for self-shielded molecular hydrogen). We have found that most of the escaping ionizing photons originates in the lowest mass galaxies with $T_{\rm vir} \lesssim 10^4$ K. Due to the shallowness of the gravitational-potential well in these galactic halos, the gas maintains a low density and its recombination rate is low. This allows the ionization front to break through the virial radius rapidly, resulting in a high escape fraction of the emitted ionizing radiation. As reionization progresses, the intergalactic medium is photo-heated and the abundance of galaxies with $T_{\rm vir} \sim 10^4$K declines, leading to a decrease in $\langle f_{\rm esc}\rangle$. This physical mechanism may account for the increase of $\langle f_{\rm esc}\rangle$ with redshift inferred by Mitra et al. (2012b).

Our study is consistent with previous studies of low mass galaxies by Wise & Cen (2009), who found a high escape fraction (> 0.1). Low mass galaxies do not form a disk (Pawlik et al. 2011), which could trap effectively ionizing photons. The relative importance of minihalos for the global production rate of ionizing photons is determined by the product $f_{esc}\times f_\star$. Here we have used a phenomenological calibration of $f_\star$. In order to produce the observed stellar density at $z = 6$–7 by minihalos, $f_\star$ has to be $\gtrsim 0.001$. This value lies in the middle range resulting from Wise & Cen (2009) idealized halo simulations, but they find the star formation efficiency in halos with $M < 10^7\,\mathrm{M}_\odot$ to be smaller. We find that the required increase of f_{esc} with redshift cannot be achieved if minihalos are sterile or form stars inefficiently.

Our simplified calculation ignored angular momentum which drives cold gas to a rotating disk configuration. Our model allowed cold gas to condense to arbitrarily small scales without making a disk, and so one might worry that it underestimates $f_{\rm esc}$. However, previous calculations have demonstrated that on the scale of galactic disks the escape fraction is very small (Wood & Loeb 2000; Gnedin et al. 2008; Razoumov & Sommer-Larsen 2006; Wise & Cen 2009), and so our inclusion of angular momentum could not increase $f_{\rm esc}$ significantly. In particular, the conclusion that $f_{\rm esc}$ is high in low-mass halos must be robust. Although our simplified model predicts zero escape fractions from brief starbursts in massive halos, the actual value of $f_{\rm esc}$ would be finite in reality due to persistent star formation histories and winds driven by supernova feedback or Lyα radiation pressure (Dijkstra & Loeb 2008). Our results are in qualitative agreement with Gnedin et al. (2008) and Razoumov & Sommer-Larsen (2006) who simulated more massive galaxies ($M \gtrsim 10^{10}\,\mathrm{M}_\odot$) and inferred an extremely small escape fraction values $f_{esc} \lesssim 1\%$), even in situations where the star formation rate is high ($\sim 10\,\mathrm{M}_\odot\ \mathrm{yr}^{-1}$). This results from the high gas densities in massive galaxies due the presence of a rotationally-supported, geometrically-thin disk.

Finally, we note that the trend we find for the increase of the escape fraction with redshift should be enhanced if

the initial mass function of stars was tilted towards more massive stars. This is because a higher production rate of ionizing photons would allow the ionization front to ionize the surrounding hydrogen blanket even faster than we calculated.

ACKNOWLEDGMENTS

Our computations were based on the Scipy open source scientific tools for Python `http://www.scipy.org/`. This work was supported in part by NSF grant AST-0907890 and NASA grants NNX08AL43G and NNA09DB30A.

REFERENCES

Barkana, R., & Loeb, A. 2001, Phys. Rep., 349, 125
Bolton, J. S., & Haehnelt, M. G. 2007, MNRAS, 382, 325
Boutsia, K., et al. 2011, ApJ, 736, 41
Bouwens, R. J., et al. 2012, ApJ, 752, L5
Caffau, E., et al. 2011, Nature, 477, 67
Cayrel, R., et al. 2004, A&A, 416, 1117
Ciardi, B., & Ferrara, A. 2005, Space Sci. Rev., 116, 625
Ciardi, B., Ferrara, A., & Abel, T. 2000, ApJ, 533, 594
Dekel, A., & Woo, J. 2003, MNRAS, 344, 1131
Dijkstra, M., Haiman, Z., Rees, M. J., & Weinberg, D. H. 2004, ApJ, 601, 666
Dijkstra, M., & Loeb, A. 2008, MNRAS, 391, 457
Dove, J. B., Shull, J. M., & Ferrara, A. 2000, ApJ, 531, 846
Fernández-Soto, A., Lanzetta, K. M., & Chen, H.-W. 2003, MNRAS, 342, 1215
Finkelstein, S. L., et al. 2012, ArXiv e-prints
Giallongo, E., et al. 2008, A&A, 482, 349
Gnedin, N. Y. 2000, ApJ, 542, 535
Gnedin, N. Y., Kravtsov, A. V., & Chen, H.-W. 2008, ApJ, 672, 765
González, V., Labbé, I., Bouwens, R. J., Illingworth, G., Franx, M., & Kriek, M. 2011, ApJ, 735, L34
Grazian, A., et al. 2011, A&A, 532, A33
Greif, T. H., Bromm, V., Clark, P. C., Glover, S. C. O., Smith, R. J., Klessen, R. S., Yoshida, N., & Springel, V. 2012, MNRAS, 424, 399
Haiman, Z., Rees, M. J., & Loeb, A. 1996, ApJ, 467, 522
Inoue, A. K., Iwata, I., & Deharveng, J.-M. 2006, MNRAS, 371, L1
Iwata, I., et al. 2009, ApJ, 692, 1287
Kitayama, T., Tajiri, Y., Umemura, M., Susa, H., & Ikeuchi, S. 2000, MNRAS, 315, L1
Kuhlen, M., & Faucher-Giguère, C.-A. 2012, MNRAS, 423, 862
Labbé, I., et al. 2010, ApJ, 708, L26
Larson, D., et al. 2011, ApJS, 192, 16
Leitherer, C., et al. 1999, ApJS, 123, 3
Loeb, A., & Furlanetto, S. 2013, The First Galaxies in the Universe (Princeton University Press, in press)
Machacek, M. E., Bryan, G. L., & Abel, T. 2001, ApJ, 548, 509
Makino, N., Sasaki, S., & Suto, Y. 1998, ApJ, 497, 555
Maselli, A., Ferrara, A., & Ciardi, B. 2003, MNRAS, 345, 379
Mesinger, A., & Dijkstra, M. 2008, MNRAS, 390, 1071
Mitra, S., Choudhury, T. R., & Ferrara, A. 2012a, MNRAS, 419, 1480
Mitra, S., Ferrara, A., & Choudhury, T. R. 2012b, ArXiv e-prints
Muñoz, J. A., & Loeb, A. 2011, ApJ, 729, 99
Navarro, J. F., Frenk, C. S., & White, S. D. M. 1997, ApJ, 490, 493
Okamoto, T., Gao, L., & Theuns, T. 2008, MNRAS, 390, 920
Pawlik, A. H., Milosavljević, M., & Bromm, V. 2011, ApJ, 731, 54
Prada, F., Klypin, A. A., Cuesta, A. J., Betancort-Rijo, J. E., & Primack, J. 2012, MNRAS, 423, 3018
Razoumov, A. O., & Sommer-Larsen, J. 2006, ApJ, 651, L89
Salvadori, S., & Ferrara, A. 2009, MNRAS, 395, L6
—. 2012, MNRAS, 421, L29
Salvaterra, R., Ferrara, A., & Dayal, P. 2011, MNRAS, 414, 847
Schneider, R., Salvaterra, R., Choudhury, T. R., Ferrara, A., Burigana, C., & Popa, L. A. 2008, MNRAS, 384, 1525
Shapley, A. E., Steidel, C. C., Pettini, M., Adelberger, K. L., & Erb, D. K. 2006, ApJ, 651, 688
Sheth, R. K., & Tormen, G. 2002, MNRAS, 329, 61
Siana, B., et al. 2007, ApJ, 668, 62
Stark, D. P., Ellis, R. S., Bunker, A., Bundy, K., Targett, T., Benson, A., & Lacy, M. 2009, ApJ, 697, 1493
Steidel, C. C., Pettini, M., & Adelberger, K. L. 2001, ApJ, 546, 665
Trac, H., & Cen, R. 2007, ApJ, 671, 1
Vanzella, E., et al. 2012a, ApJ, 751, 70
—. 2012b, MNRAS, 424, L54
Wise, J. H., & Cen, R. 2009, ApJ, 693, 984
Wood, K., & Loeb, A. 2000, ApJ, 545, 86
Wyithe, J. S. B., & Loeb, A. 2003, ApJ, 586, 693